DESIGN AND OPTIMIZATION OF DC SQUIDS FABRICATED USING A SIMPLIFIED FOUR-LEVEL PROCESS

R. Cantor, T. Ryhänen*, D. Drung, and H. Koch
Physikalisch-Technische Bundesanstalt, Institut Berlin,
Abbestr. 10-12, D-1000 Berlin 10, FRG
*on leave from: Helsinki University of Technology,
Otakaari 5A, SF-02150 Espoo, Finland

H. Seppä
VTT Metrology Research Institute, Technical Research Center of Finland,
Otakaari 7B, SF-02150 Espoo, Finland

Abstract

We describe an optimization procedure which we have used to design two types of ultralow noise dc Superconducting Quantum Interference Devices (SQUIDs) with integrated flux coupling circuits, a magnetometer and a gradiometer. Essential to this design approach is the reduction of the parasitic capacitance, the choice of a layout which moves the input coil resonances well away from the desired operating frequency of the SQUID, and the proper damping of these resonances. We show that both the microwave and LC resonances can be damped in a nearly noise-free manner by placing an RC shunt in parallel with the input coil. This leads to smooth voltage-flux modulation characteristics and significantly improved noise performance. A simple, four-level $Nb/Si_xN_y/Nb$ Josephson junction technology is described for device fabrication. White flux noise levels of $5 \times 10^{-7}\Phi_0/\sqrt{Hz}$ for the magnetometer and $7.9 \times 10^{-7}\Phi_0/\sqrt{Hz}$ for the gradiometer have been measured. The corresponding uncoupled energy resolutions are 100 $\hbar$ and 130 $\hbar$, respectively. The $1/f$ noise of the magnetometer at 1 Hz is less than $4 \times 10^{-6}\Phi_0/\sqrt{Hz}$.

Introduction

Considerable effort has been devoted to the design of dc superconducting quantum interference devices (SQUIDs) having noise energies approaching the quantum limit. Such devices have been designed and built, but in order to be useful for practical applications coupling to the very low SQUID inductance is necessary. The use of a square-shaped washer for the SQUID loop with a closely coupled, integrated input coil[1] largely solves this problem but introduces numerous parasitic effects which, if not taken into account in designing the SQUID, can lead to strong irregularities in the current-voltage ($I - V$) characteristics and to a significant deterioration of the ultimate noise performance[2,3]. Knuutila et al.[4] have developed a design approach for the optimization of low noise SQUIDs with integrated coupling circuits which takes these parasitic effects into account. In this paper, we first summarize the parasitic effects introduced by the input circuit and describe the design principles which we have followed to optimize two different types of ultralow noise dc SQUIDs with integrated flux coupling circuits, a magnetometer and a gradiometer. This is followed by a brief description of the simple, four-level process which we have used to fabricate these sensors and a discussion of the measured noise performance.

SQUID design principles

Standard design principles for the optimization of dc SQUIDs without flux coupling circuits require[5] $\beta_c = 2\pi I_c R^2 C/\Phi_0 \lesssim 1$ and $\beta = 2LI_c/\Phi_0 \approx 1$, where I_c is the critical current per junction, R is the junction shunt resistance, C is the junction capacitance, L is the SQUID inductance, and Φ_0 is the flux quantum. In this case, it is well known that the energy resolution of the SQUID $\epsilon \propto \sqrt{LC}$ so low values for L and C are desirable. For a dc SQUID with an integrated flux coupling circuit, the presence of the input coil introduces a parasitic capacitance C_p. A high C_p diminishes the damping of the system and, according to recent simulations[3,6,7], leads to hysteretic characteristics. We show elsewhere[7] that the energy resolution is reduced, scaling as $\sqrt{1 + 2C_p/C}$ for $C_p \lesssim 4C$.

Manuscript received September 24, 1990.

For $C_p \gg C$, the reduction is even stronger. Thus, the SQUID should be designed so as to minimize C_p. This can be done by reducing the size of the washer, reducing the input coil length and linewidth, and using a low permittivity dielectric for the insulator between the input coil and the washer.

The presence of the input coil can also lead to a variety of resonances, such as the LC resonance involving the inductance of the input coil and its lumped capacitance to the SQUID washer, the microwave transmission line resonance formed by the microstripline comprising the input coil and the washer, and an enhancement of the $\lambda/2$ resonance of the washer[2,4,8,9,10]. By reducing the size of the washer and input coil as described above, the washer resonance occuring at the frequency f_{washer} be can be moved to frequencies much higher than the intended operating frequency of the SQUID, f_{op}. However, a short input coil causes the LC resonance at low frequencies to move towards f_{op}. In addition, if the length of the input coil becomes too short, the microstripline resonance occuring at the frequency f_{strip} can approach f_{op}. Thus, a design compromise must be made. The input coil should be made long enough in order to move the transmission line resonance to frequencies well below f_{op}. Increasing the length of the input coil also effectively reduces the cutoff frequency of the frequency dependent coupling constant so the Josephson oscillations are less likely to activate the resonances in the flux coupling circuit.

In addition to moving the resonances well away from f_{op}, they should be damped if possible. Otherwise, thermally activated transitions between the different states will lead to enhanced noise[2]. The use of a damping resistor across the SQUID inductance has been shown to be effective in smoothing the SQUID characterisitics and improving performance[11,12] but the resistor introduces additional noise as well. The insertion of a series R_xC_x shunt in parallel with the input coil was proposed[2] to damp the low frequency resonances. In this way, the noise contribution is minimal. In addition, the R_xC_x shunt serves as a rf filter. The motivation for the shunt is essentially based on a reduction of the time spent in the resonant state. Subsequent experiments have confirmed the effectiveness of an R_xC_x shunt in smoothing SQUID characteristics and in improving noise performance[13].

The ideas discussed above have been used to design a very low noise SQUID with intermediate coupling transformer[4]. However, the input coil microstripline was terminated using a resistor rather than a series resistor-capacitor shunt. The effects of parasitic capacitance were not correctly taken into account and the SQUID was overdamped. Also, the design of the SQUID was rather complex and the fabrication process required 11 mask levels.

In view of the above discussion, we have chosen to use the following simple principles for the design of dc SQUIDs with integrated flux coupling circuits:

- The SQUID layout and fabrication process are chosen so that $C_p \lesssim C$.
- The size of the SQUID is chosen so that $f_{strip} < f_{op}/4$ and $f_{washer} > 4f_{op}$. This ensures that the resonant frequencies are located well away from the intended operating frequency.
- The capacitor C_x is chosen so that the input coil LC resonance at the frequency $f_{input} \ll f_{op}$ in order to prevent the Josephson oscillations from activating this resonance.
- The resistor R_x is chosen to match the nominal impedance of the input coil microstripline in order to properly terminate

0018-9464/91/0300-2927$01.00

the transmission line. The capacitor C_x is effectively a short at these frequencies.

- The Q value of the input circuit resonance must be low in order to reduce the "lifetime" of the resonant state, but high enough to prevent the Josephson oscillations from mixing the noise down to low frequencies (for our devices $Q \approx 4$).
- The overall design should be simple and require a minimum number of process steps in order to increase device yield.

Optimization

An effective scheme for the optimization of dc SQUIDs was first presented by Knuutila et al.[4]. We have improved this scheme by properly taking into account the functional dependence of the energy resolution on C_p. If the various microwave resonances are moved to frequencies well away from $f_{\rm op}$ and are damped as discussed above, it has been shown that the external energy resolution of a dc SQUID with flux coupling circuit, defined as $\epsilon_{\rm ext} = (B_n A_{\rm eff})^2/2L_p$, where B_n is the field noise and $A_{\rm eff}$ is the effective area of the pick-up loop with inductance L_p, may be expressed as[4]

$$\epsilon_{\rm ext} = \frac{\{L_p/L_i + (1-k_s^2 s)\}^2}{L_p/L_i}\frac{\langle\Phi_n^2\rangle}{2k_s^2 L} \quad . \tag{1}$$

Here, L_i is the inductance of the input coil, k_s is the coupling constant, s is a factor which describes the screening of the input coil inductance by the SQUID[4], and $\langle\Phi_n^2\rangle^{1/2}$ is the flux noise. The equivalent intrinsic flux noise can be expressed as[7,10]

$$\langle\Phi_n^2\rangle = 2k_BT\left\{\frac{L^2}{R} + \frac{2R_{\rm dyn}}{(\partial\bar{V}/\partial\Phi_a)^2}\right\}\left\{1+\frac{2C_p}{C}\right\}^{1/2} \quad . \tag{2}$$

Here, $R_{\rm dyn}$ is the dynamic resistance of the SQUID and $\partial\bar{V}/\partial\Phi_a$ is the forward voltage-flux transfer function. Using the approximations $R_{\rm dyn} \approx R/\sqrt{2}$, $\partial\bar{V}/\partial\Phi_a \approx 2RI_c/\Phi_0(1+\beta)$, and the fixed value $\beta_c = 0.7$, it has been shown[4,10] that the theoretical optimum of $\epsilon_{\rm ext}$ is obtained with $\beta = 2.6$, $k_s = 0.83$ and $L_p/L_i = 0.88$. In practice, ϵ_{ext} is optimized by varying the SQUID dimensional parameters (such as the washer hole size and junction area), the critical current density, the junction shunt resistance, and the number of input coil turns, in order to determine the parameters β_L, k_s, and L_p/L_i. The optimization is subject to process constraints which limit the feasable range of film thicknesses and widths and the constraint that the resonant frequencies be located well away from $f_{\rm op}$ as discussed above. The parameter L_p/L_i in effect determines L_p, since the constraint imposed by the resonances fixes L_i. The constrained optimization of a given design may lead to a set of design parameters which necessarily deviate somewhat from the optimal values according to theory given above. However, the minimum of the energy resolution is rather broad so some deviation can be tolerated without significantly affecting the ultimate performance.

Once the SQUID dimensions and electrical parameters have been generated, the next step is to determine the optimal chip size. This is an iterative process. A trial chip size is chosen and, for a magnetometer, the field noise B_n is optimized; for a gradiometer, the field gradient noise $G_n = B_n/b$, where b is the gradiometer baseline, is optimized. The optimization is carried out by varying the pick-up loop linewidths to minimize the ratio of the pick-up loop inductance to the effective loop area. The constraint is that the pick-up loop inductance be comparable to L_p determined above. Here, an application dependant compromise can be made. By tolerating an inductance mismatch, some improvement in field resolution may be achieved at the expense of a reduced energy resolution.

Device fabrication

All of the sensors to be described below have been fabricated using a simple, four-level $Nb/Si_xN_y/Nb$ Josephson junction technology which has been described elsewhere in detail[14,15]. Briefly, the process is carried out as follows:

- A $Nb/Si_xN_y/Nb$ trilayer is deposited over an entire 2 inch Si wafer and patterned to define the SQUID washer (with a $2-3$ μm slit width), the pick-up loops, and the capacitors C_x using a wet etch process.
- The junctions (typically 5×5 μm^2) and several high critical current contacts to provide zero-voltage connections to the base electrode are defined by protecting the junction and contact areas with photoresist and then anodizing all of the remaining areas of the upper Nb film. The upper Nb films of the capacitors are also anodized. The high critical current contacts are used, for example, to connect the junction shunts and for routing the input coil current return path through the SQUID washer. In order to reduce the parasitic capacitance an additional Si_3N_4 insulation layer is then deposited through the anodization mask and lifted off. The dielectric for the capacitors therefore consists of a Nb_2O_5/Si_3N_4 bilayer.
- The Pd shunt resistor layer is deposited and patterned using a lift-off stencil.
- A Nb layer is deposited and patterned, also using a lift-off stencil, to define the input coil (3 μm linewidth), capacitor top plates, and interconnects.

With this limited number of process steps it is not possible to cover the slit in order to reduce stray inductance. This effectively limits the minimum SQUID inductance that can be fabricated. In spite of this limitation we show below that it is possible to fabricate ultralow noise devices using this simple process.

Sensor design and performance

We have designed and built two types of sensors using the guidelines, optimization procedure, and fabrication process described above, a magnetometer and a gradiometer. Since the design principles for both sensors are similar, we present only the magnetometer results in detail and only summarize the results for the gradiometer.

The complete magnetometer has been integrated on a 4×4 mm^2 chip. A total of 105 chips are fabricated from a single 2 inch Si wafer. A micrograph of the magnetometer SQUID area is shown in Fig. 1.

We report here on the effectiveness of the R_xC_x shunt in improving noise performance. A complete characterisation of this magnetometer will be presented elsewhere. For these experiments, a series of magnetometers having different values of the shunt resistor R_x were fabricated. Presented here are the measured data for two magnetometers from this series. Both are from the same wafer and have nearly identical I_c and R; the SQUID of one of the magnetometers has an R_xC_x across its input coil, optimized according to the guidelines above, the other does not. The pa-

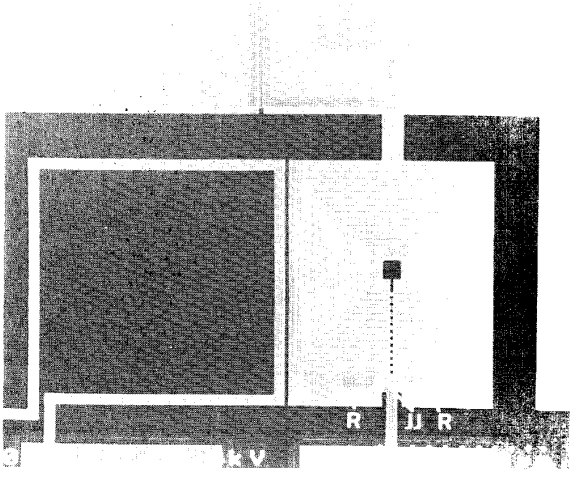

Figure 1. Micrograph of the magnetometer SQUID area. The Josephson junctions (JJ), junction shunts (R), R_xC_x shunt resistor (R_x) and capacitor (C_x) are indicated. C_x has been integrated into the pick-up loop.

rameters of the R_xC_x shunt are $R_x = 6.5\ \Omega$ and $C_x = 30$ pF. In Fig. 2, the measured $I-V$ characteristics of both magnetometers are shown. From these curves, it can be seen quite clearly that the R_xC_x shunt removes the feature which arises around 10 μV. We attribute this feature to be due to the microstripline resonance. The resonance is a $\lambda/4$ resonance in this case, since one end of the input coil is grounded in this design. From the known geometry of the coil, this corresponds to 3 GHz or 6 μV, which is consistent with the data. The absence of a proper termination leads to a high Q resonance, hence the strong feature in the $I-V$ characteristic. In addition, a very small feature can be seen near 40 μV which may be due to an effective capacitance[7] that is a function of C_p and C; such a feature should occur near this voltage for $C_p \approx 0.9$ pF, which is close to what we estimate for this device. The very sharp step near 85 μV is the washer resonance which is not separately damped. The corresponding voltage-flux ($V-\Phi$) modulation curves for the two magnetometers are shown in Fig. 3. The characteristics of the magnetometer without an R_xC_x shunt across the SQUID input coil exhibit severe irregularities due to switching events between the different states, whereas the magnetometer with an optimized R_xC_x shunt has nearly ideal characteristics. Thus, this magnetometer is ideally suited for flux modulation or positive feedback[16,17] read-out schemes which require smooth characteristics for optimum performance and easy operation.

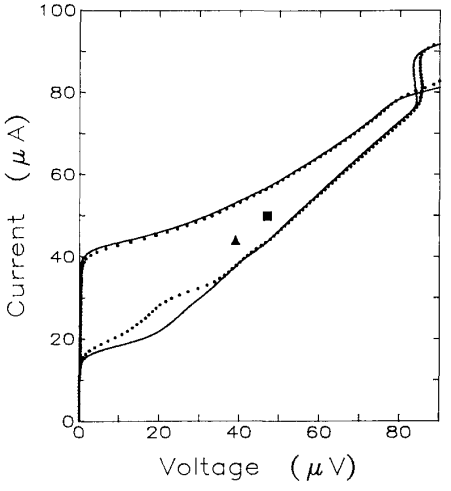

Figure 2. Measured current-voltage characteristics for two different magnetometers having nearly identical I_c and R, one without an R_xC_x shunt (dotted curve), the other with an R_xC_x shunt in parallel with the SQUID input coil (full curve). For the lower curve, the applied flux $\Phi_a = (n+1/2)\Phi_0$; for the upper curve, $\Phi_a = n\Phi_0$. The working points at which the white flux noise was measured to be optimum are indicated by (■) without R_xC_x shunt, (▲) with R_xC_x shunt.

The noise performance of the magnetometers was measured using a directly coupled SQUID magnetometer[18] as a preamplifier. For these measurements, both chips were enclosed by a single Pb shield. The voltage signal from the magnetometer SQUID was coupled to the preamplifier via two 10 Ω resistors and a Cu wirewound coil. With the magnetometer at a given working point, the noise at the preamplifier output was measured using a spectrum analyser. The preamplifier noise, dominated by the Johnson noise of the resistors, was measured separately and used to reduce the magnetometer spectra in order to determine the intrinsic noise of the magnetometer.

The equivalent flux noise spectral density of the magnetometer with the optimized R_xC_x shunt is shown in Fig. 4. The working point used for this measurement is indicated by a triangle in Fig. 2. The white flux noise $5\times10^{-7}\Phi_0/\sqrt{\text{Hz}}$ corresponds to uncoupled and coupled energy resolutions of 99 $\hbar$ and 138 $\hbar$, respectively. This is to be compared with the theoretical value of $4.7\times10^{-7}\Phi_0/\sqrt{\text{Hz}}$ according to the optimization calculations. The $1/f$ corner frequency is 40 Hz and the flux noise at 1 Hz

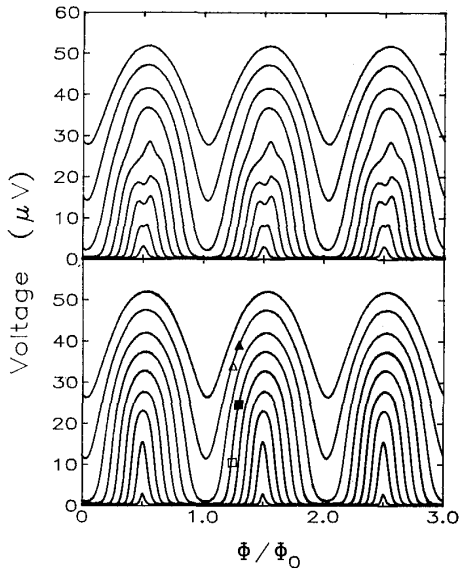

Figure 3. Voltage-flux modulation characteristics measured for several different bias current settings for two magnetometers having nearly identical I_c and R; (a) without R_xC_x shunt, (b) with R_xC_x shunt. In (b), the indicated working points and corresponding measured white flux noise data are as follows:
(▲) $I_c = 44\ \mu$A, $\Phi_a = 1.3\Phi_0$, $\langle\Phi_n^2\rangle^{1/2} = 5\times10^{-7}\Phi_0/\sqrt{\text{Hz}}$;
(△) $I_c = 44\ \mu$A, $\Phi_a = 1.25\Phi_0$, $\langle\Phi_n^2\rangle^{1/2} = 5.9\times10^{-7}\Phi_0/\sqrt{\text{Hz}}$;
(■) $I_c = 36\ \mu$A, $\Phi_a = 1.3\Phi_0$, $\langle\Phi_n^2\rangle^{1/2} = 5.5\times10^{-7}\Phi_0/\sqrt{\text{Hz}}$;
(□) $I_c = 36\ \mu$A, $\Phi_a = 1.25\Phi_0$, $\langle\Phi_n^2\rangle^{1/2} = 6.5\times10^{-7}\Phi_0/\sqrt{\text{Hz}}$.

is $3.8\times10^{-6}\Phi_0/\sqrt{\text{Hz}}$. For these measurements, the magnetometer was not flux-locked. The noise of this magnetometer has also been measured at several other working points; these results are summarized in Fig. 3. From these data, it can be seen that the flux noise does not change significantly as the working point is moved. Also, it should be noted that the best noise performance does not correspond to a point of maximum gain, where excess noise caused by the microwave resonances is present.

The working point at which the white flux noise of the magnetometer without an R_xC_x shunt was measured to be optimum is indicated by a square in Fig. 2. For this sensor, we measured a white flux noise of $7.8\times10^{-7}\Phi_0/\sqrt{\text{Hz}}$. Here it can be seen that,

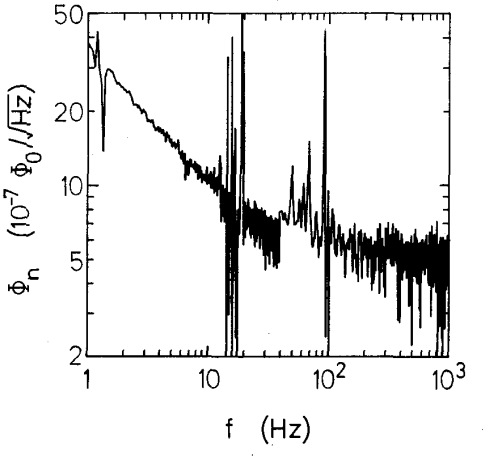

Figure 4. Measured equivalent flux noise spectral density for a magnetometer with an R_xC_x shunt ($R_x = 6.5\ \Omega$, $C_x = 30$ pF) in parallel with the SQUID input coil after subtracting the preamplifier noise contribution. The various peaks are due to mechanical resonances in the dewar.

for optimum performance, the magnetometer without an R_xC_x must be operated at higher bias current due to the presence of the undamped microstripline resonance. Although the measured white flux noise for the undamped magnetometer is very low, the resonance limits the useful operating range of the sensor. We have measured the flux noise of a third magnetometer for which the shunt resistor $R_x = 0.5\ \Omega$. Although the white flux noise of this magnetometer, $5.4 \times 10^{-7}\Phi_0/\sqrt{\text{Hz}}$, is close to that measured for the magnetometer with an optimized R_xC_x shunt, the voltage-flux characteristics for this magnetometer were not completely smooth. Further experiments are underway to determine the dependence of the flux noise on R_x.

The magnetometer was calibrated in the Berlin Magnetically Shielded Room (BMSR) using a Helmholtz coil. For these measurements, a Pb shield was not used. The measured field sensitivity $B/\Phi_a = 6.1\ \text{nT}/\Phi_0$ corresponds to a white field noise $B_n = 3.1\ \text{fT}/\sqrt{\text{Hz}}$. For this series of magnetometers the pick-up loop geometry was optimized to satisfy inductance matching. By tolerating an inductance mismatch, our optimization model indicates that a sensitivity of $5\ \text{nT}/\Phi_0$ can be achieved. This would lead to an ultimate field noise of $2.5\ \text{fT}/\sqrt{\text{Hz}}$. Magnetometers of this type are currently being built. The measured parameters of the magnetometer with the nominally optimized R_xC_x shunt are summarized in Tab. 1. Altogether, the performance of this magnetometer is excellent, especially for a sensor of this size and simplicity.

Depicted in Fig. 5, the gradiometer has an overall chip size of $11 \times 17\ \text{mm}^2$ and a baseline of 10.2 mm. The chip size was chosen so as to be compatible with sensor inserts currently in use at our institute[19]. An equivalent circuit diagram for the gradiometer is shown in Fig. 6.

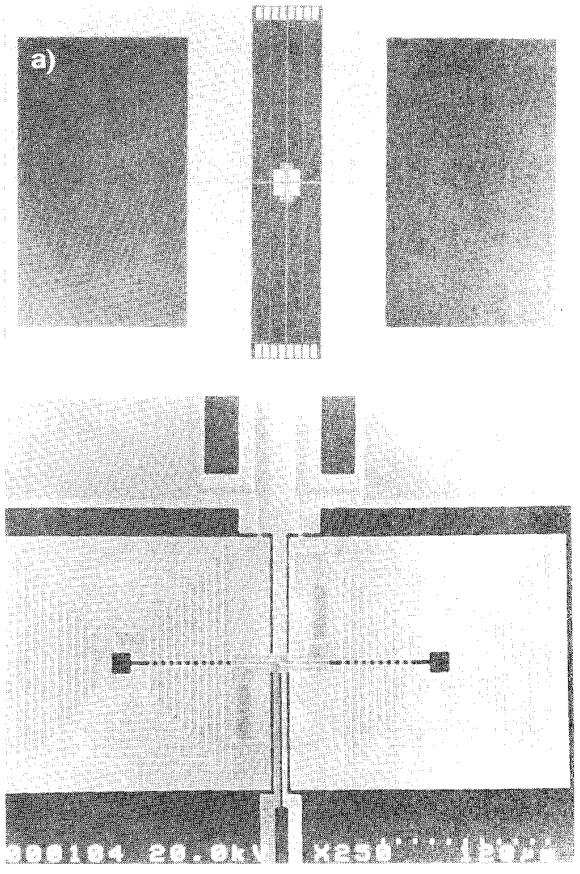

Figure 5. Micrographs of (a) the gradiometer chip and (b) the gradiometer double washer SQUID. Each side of the input coil is connected to a series resistor($R_x/2$)-capacitor($2C_x$) shunt to ground.

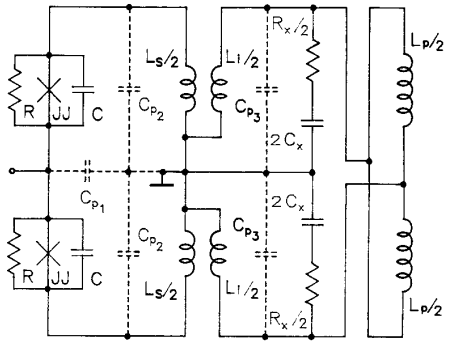

Figure 6. Equivalent circuit diagram of the gradiometer. Here, C_{p1} is the parasitic capacitance arising from the overlap of the voltage leads and C_{p2} and C_{p3} are the distibuted parasitic capacitances associated with the washer and input coil.

The measured $I - V$ and $V - \Phi$ modulation curves for the gradiometer are shown in Fig. 7 and 8, respectively. The features in the $I - V$ characteristics are similar to those observed for the magnetometer and the $V - \Phi$ characteristics are smooth for the range of bias currents where the device is to be operated.

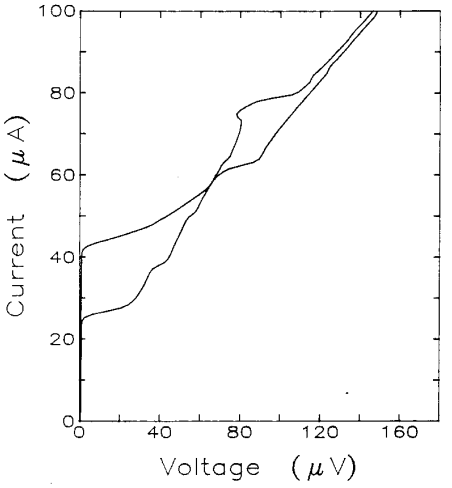

Figure 7. Current-voltage characteristics of the gradiometer measured for $\Phi_a = (n + 1/2)\Phi_0$ and $\Phi_a = n\Phi_0$.

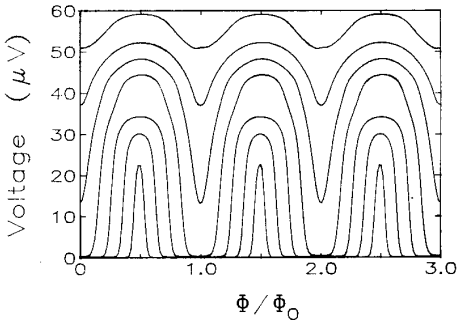

Figure 8. Voltage-flux modulation characteristics of the gradiometer measured for several different bias current settings.

The flux noise of the gradiometer was measured using the same procedure described above for the magnetometer. The measured white flux noise $7.9 \times 10^{-7}\Phi_0/\sqrt{\text{Hz}}$ corresponds to uncoupled and coupled energy resolutions of 131 $\hbar$ and 182 $\hbar$, respectively. The theoretical flux noise is $7 \times 10^{-7}\Phi_0/\sqrt{\text{Hz}}$ according to the optimization calculations.

The gradiometer was calibrated in the BMSR using a long wire. The field gradient required to produce one flux quantum in the SQUID was integrated over the area of the pick-up loops to determine the gradient sensitivity 140 $\text{nT/m}\Phi_0$. This together with the measured flux noise given above implies a gradient noise of 110 $\text{fT/m}\sqrt{\text{Hz}}$. The measured gradiometer parameters are summarized in Tab. 1.

Table I. Measured parameters and performance for two example devices.

Parameter	Magnetometer	Gradiometer
L	51 pH	97 pH
C	1 pF	1 pF
I_c	20 μA	20 μA
R	2.4 Ω	3 Ω
L_i	6 nH	8.4 nH
L_p	5.5 nH	8.5 nH
R_x	6.5 Ω	11.4 Ω
C_x	30 pF	30 pF
β	1	1.9
β_c	0.6	1.2
k_s	0.85	0.85
$\langle\Phi_n^2\rangle^{1/2}$	$5.0 \times 10^{-7}\Phi_0/\sqrt{\text{Hz}}$	$7.9 \times 10^{-7}\Phi_0/\sqrt{\text{Hz}}$
$\epsilon_{\text{uncoupled}}$	99$\hbar$	131$\hbar$
$\epsilon_{\text{coupled}}$	138$\hbar$	182$\hbar$
B/Φ_a	6.1 nT/Φ_0	-
$(\partial B/\partial x)/\Phi_a$	-	140 $\text{nT/m}\Phi_0$
B_n	3.1 $\text{fT}/\sqrt{\text{Hz}}$	-
G_n	-	110 $\text{fT/m}\sqrt{\text{Hz}}$

Conclusions

We have presented a concise set of guidelines for the design and optimization of dc SQUIDs with integrated flux coupling circuits. Following these guidelines, we have designed and built two types of sensors, a magnetometer and a gradiometer; both were fabricated using a simple, four-level $\text{Nb/Si}_x\text{N}_y\text{/Nb}$ Josephson junction technology. We have demonstrated the effectiveness of an R_xC_x shunt in parallel with the SQUID inductance in smoothing the characteristics and improving noise performance. Both sensors have exceptionally low noise, indicating the success of the design and optimization procedure. This procedure should be useful for the design of other high performance SQUIDs with arbitrary pick-up loop configurations.

This work has been supported by the German Federal Ministry of Economic Affairs (BMWi) under contract 9303. One of the authors (T.R.) gratefully acknowledges support from the Academy of Finland.

References

[1] M.B. Ketchen and J.M. Jaycox, Appl. Phys. Lett. **40**, 736 (1982).
[2] H. Seppä and T. Ryhänen, IEEE Trans. Magn. **MAG-23**, 1083 (1987).
[3] D. Drung and W. Jutzi, in: SQUID'85, Superconducting Quantum Interference Devices and Their Applications, eds. H.D. Hahlbohm and H. Lübbig (Walter de Gruyter, Berlin, 1985),p. 807.
[4] J. Knuutila, M. Kajola, H.Seppä, R. Mutikainen and J. Salmi, J. Low Temp. Phys. **71**, 369 (1988).
[5] C.D. Tesche and J. Clarke, J. Low Temp. Phys. **29**, 301 (1977).
[6] J.A. Ketoja, J. Kurkijärvi, and R.K. Ritala, Phys. Rev. **B30**, 3757 (1984).
[7] T. Ryhänen, R. Cantor, D. Drung, H. Koch, and H. Seppä, this volume.
[8] C. Hilbert and J. Clarke, J. Low Temp. Phys. **61**, 237 (1985).
[9] B. Muhlfelder, J.A. Beall, M.W. Cromar, R.H. Ono, and W.W. Johnson, IEEE Trans. Magn. **MAG-21**, 427 (1985).
[10] T. Ryhänen, H. Seppä, R. Ilmoniemi, and J. Knuutila, J. Low Temp. Phys. **76**, 287 (1989).
[11] K. Enpuku, K. Yoshida, and S. Kohjiro, J. Appl. Phys. **60**, 4218 (1986).
[12] V. Foglietti, W.J. Gallagher, M.B. Ketchen, A.W. Kleinsasser, R.H. Koch, and R.L. Sandstrom, Appl. Phys. Lett. **55**, 1451 (1989).
[13] J. Knuutila, A. Ahonen, and C. Tesche, J. Low Temp. Phys. **68**, 269 (1987).
[14] R. Cantor, D. Drung, M. Peters, H.J. Scheer, and H. Koch, Supercond. Sci. Technol. **3**, 108 (1990).
[15] R. Cantor, D. Drung, M. Peters, and H. Koch, J. Appl. Phys. **67**, 3038 (1990).
[16] D. Drung, R. Cantor, M. Peters, T. Ryhänen, and H. Koch, this volume.
[17] H. Seppa, A. Ahonen, J. Knuutila, J. Simola, and V. Vilkman, this volume.
[18] D. Drung, R. Cantor, M. Peters, H.J. Scheer, and H. Koch, Appl. Phys. Lett. **57**, 406 (1990).
[19] H. Koch, R. Cantor, D. Drung, S.N. Erne, K.P. Matthies, M. Peters, T. Ryhänen, H.J. Scheer, and H.D. Hahlbohm, this volume.